Robotica (2023), **41**, pp. 2735–2753
doi:10.1017/S0263574723000632

CAMBRIDGE UNIVERSITY PRESS

RESEARCH ARTICLE

Design, static analysis, and dynamic system modeling of 3-PPRS parallel manipulator with load-balancing UPS leg

A. Xavier Reni Prasad and M. Ganesh

School of Mechanical Engineering, SASTRA Deemed to be University, Tamil Nadu, India
Corresponding author: A. Xavier Reni Prasad; Email: xavierreniprasad@sastra.ac.in

Received: 31 January 2023; **Accepted:** 22 April 2023; **First published online:** 22 May 2023

Keywords: parallel manipulators; end effector; load balancing mechanism; robot dynamics; damper element; 3-PPRS; a passive damper mechanism; mathematical model; vibration; stiffness

Abstract

As a heavy load is applied to the parallel manipulators, it causes inaccuracies while positioning the end-effector or unbalanced dynamic forces in the legs. Various load-balancing techniques overcome this. However, the disadvantage of most load-balancing mechanisms is that they add inertia to the assembly and decrease the speed of motion. This article studies a new load-balancing method (a passive damper mechanism). The passive balancing mechanism is proposed to negate the inertia effects while countering the static inaccuracies in the parallel mechanism. This is verified by the structural analysis of the mechanism. The impact of the damper element on the dynamics of the mechanism is unknown. Hence, a complete mathematical model for the balancing mechanism has been developed to study its impact on the dynamics of the entire structure. Laplace transformations characterize the system response. The inclusion of a passive damper in a 3-prismatic-prismatic-revolute-spherical system was examined and found to be stable and critically damped. Such a passive damper was envisaged to facilitate additional force transmission for the actuators, and the DC gain from the system response validates the torque support for the actuators.

1. Introduction

Spatial parallel manipulators should be balanced properly, that is, stable in all configurations. Different balancing mechanisms were developed by researchers two decades back. Examples are counterweight [1, 2], pneumatic or hydraulic cylinders [3], mechanical balancing like gear train [4], helical/torsional spring [5, 6], and cam mechanism [7]. Most of the above-mentioned balancing mechanisms were used for planar mechanisms. However, when it comes to spatial mechanisms where the center of mass is high above the platform, parallelogram mechanisms [8, 9] are used for gravity compensation. Arakelian [10] used the pantograph mechanism, a special case of parallelogram mechanism, to address the balancing of a spatial parallel manipulator. A geometric method for the static balancing of spatial mechanisms was proposed by Wang [11]. Dynamic balancing methods were categorized as balancing before kinematic synthesis and balancing after the design by Zhang [12].

All the above-mentioned balancing mechanisms solely address the balancing issue. While incorporating balancing mechanisms, an increase in the mass of the assembly cannot be avoided with the above methods, and hence the actuator force requirements are increased subsequently. If the mass of the balancing mechanism is reduced, the damping of forces becomes challenging. Hence, while designing a balancing mechanism, damping needs to be also taken into account. This article proposes a lightweight balancing mechanism that does not sacrifice damping. In addition to load balancing, it can also address force requirements.

1.1. Three-legged decoupled parallel manipulators

Decoupled parallel manipulators with three legs have two active joints and two passive joints in each leg, leading to six actuators and hence 6-degrees of freedom (DOF). For example, the first

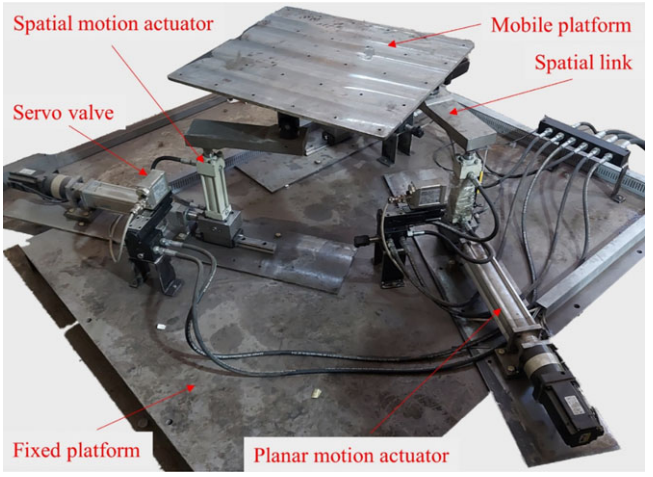

Figure 1. *The 3-PPRS parallel manipulator (equipment developed in-house).*

two joints are actuated in each leg in the case of a 3-prismatic-prismatic-revolute-spherical (PPRS) manipulator.

The first actuator from each leg collectively produces a 3-DOF planar motion, either translational along the X-Y plane or rotational motion about the Z axis. Similarly, the second actuator from each leg collectively produces a 3-DOF spatial motion which is either translational motion along the Z axis or rotational motion about the X and Y axes (Fig. 1). Hence, the set of actuators that are causing translation in X-Y plane and rotational motion in X-Y plane are grouped as *planar motion actuators*. Similarly, the set of actuators causing rotational motion about the X and Y axes and translation along the Z axis are grouped as *spatial motion actuators* [13].

The 3-PPRS parallel manipulator without the load-balancing mechanism is shown in Fig. 1. It is a three-legged decoupled parallel manipulator having a fixed platform connected to a mobile platform through three identical actuator legs. Each leg comprises a horizontal motion actuator, a vertical motion actuator, and a link with a revolute joint at one end and a spherical joint at the other.

Such manipulators are called decoupled because the manipulator can exhibit planar and spatial motion separately, using a limited number of actuators (three actuators in each case). The role of transmission links in this parallel manipulator is mainly for transmitting the planar motion in the X-Y plane. However, the planar links cause cantilever action, which affects the stiffness and result in inaccuracies due to the thrust forces on the mobile platform. It is a common load-balancing challenge experienced by planar manipulators, similar to the load-balancing issue in serial manipulators.

Hence, the links are made spatial as in the case of general spatial manipulators (Stewart platform or delta manipulators), where the transmission links elevate the mobile platform from the base platform. The spatial links are created without changing the axes of the joints. It means the force transmission will still be retained in the X-Y plane (Fig. 1). Due to spatial links, the improvement in translational stiffness was reported in [14] despite the reduced force transmission in the X-Y plane.

However, such inclusion of spatial links was insufficient and resulted in deflection due to the heavy payload. The deflection of the entire assembly of the developed in-house prototype is displayed in Fig. 2. Such deflections can be vastly subdued by removing the manufacturing and assembly tolerances. However, the loading impact affecting the stiffness is evident, causing strain on the actuators and producing errors due to lateral deformations of actuator assemblies [15].

From the above argument and based on the discussion in Section 1.1, it can be well established that any improvement in the method of balancing upsurges the torque of the actuator. To address this issue, it has been proposed to add a passive damper in the load-balancing UPS leg (Fig. 3), which provides force compensation along with load balancing. While adding a damper element with reduced mass, it is essential to verify the structural analysis results.

https://doi.org/10.1017/S0263574723000632 Published online by Cambridge University Press

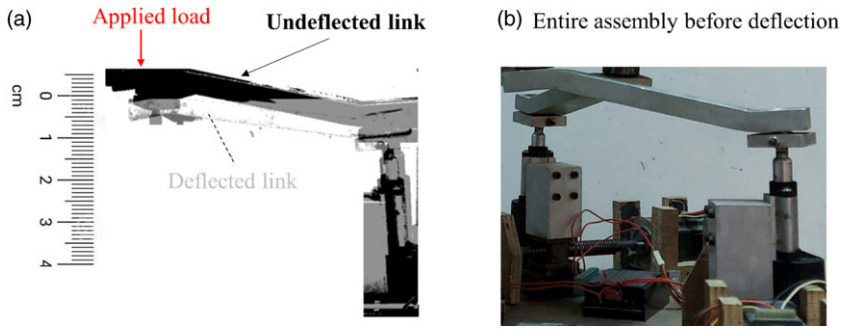

Figure 2. *(a) Deflection of entire assembly on the application of external load on top of the mobile platform of 3-PPRS manipulator and (b) entire assembly without external load on mobile platform-without deflection (prototype developed in-house).*

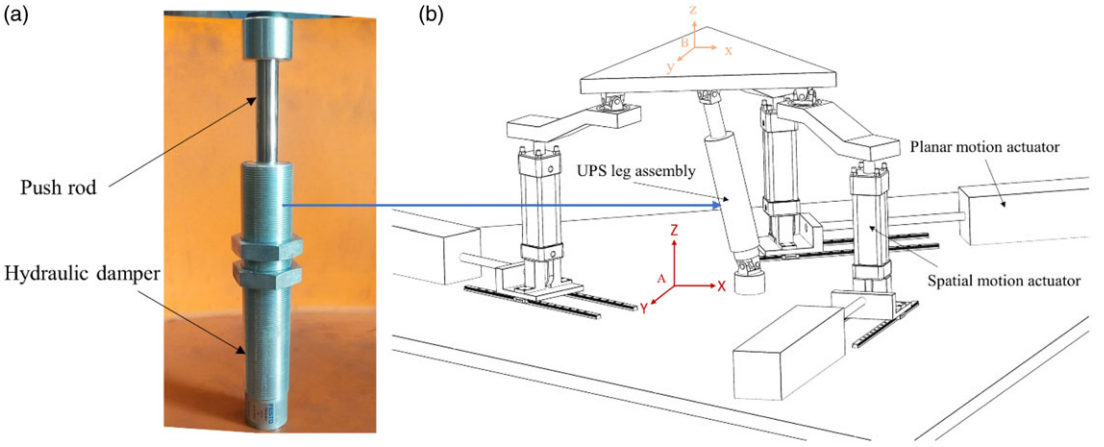

Figure 3. *(a) Festo shock absorber as a passive damper element and (b) the 3-PPRS manipulator with passive damper element.*

A passive damper element is used for the prismatic link in the UPS configuration. Adding the damper element to the parallel manipulator resembles a semi-active damper in the suspension system [16]. The main functioning difference between an actuator in the suspension system and the damper in parallel manipulators is as follows. The role of the actuator in the suspension system is to provide timely reaction forces to counteract the input forces and additionally dissipates part of the vibration energy. A damper's main role in a shake table is to suppress/dissipate vibrations due to reactive forces and additionally provide counteracting forces to the gravity load. However, the forces are non-linear in the case of the damper.

Many configurations of serial structures can be utilized as a load-balancing leg [17]. The universal-prismatic-universal (UPU) leg is preferred among such configurations due to minimal interference and avoids singularities. However, the drawback of UPU leg assembly is that it constrains the workspace and the DOF [18]. Hence, a UPS configuration is preferred, and singularity point in the workspace is carefully avoided [19].

In what follows, the Denavit–Hartenberg methodology for the UPS leg in Section 2 followed by the demonstration of stiffness addition to the parallel mechanism through Jacobian analysis of the UPS leg configuration in Section 3. Structural analysis is also done to verify the improvement in the load balancing, and the results are compared with three different architectures of the 3-PPRS parallel manipulator in Section 4. The impact of the damper mechanism on the passive leg is studied using detailed dynamic system modeling in Section 5. The system modeling is done for a single-leg assembly to illustrate the concept.

https://doi.org/10.1017/S0263574723000632 Published online by Cambridge University Press

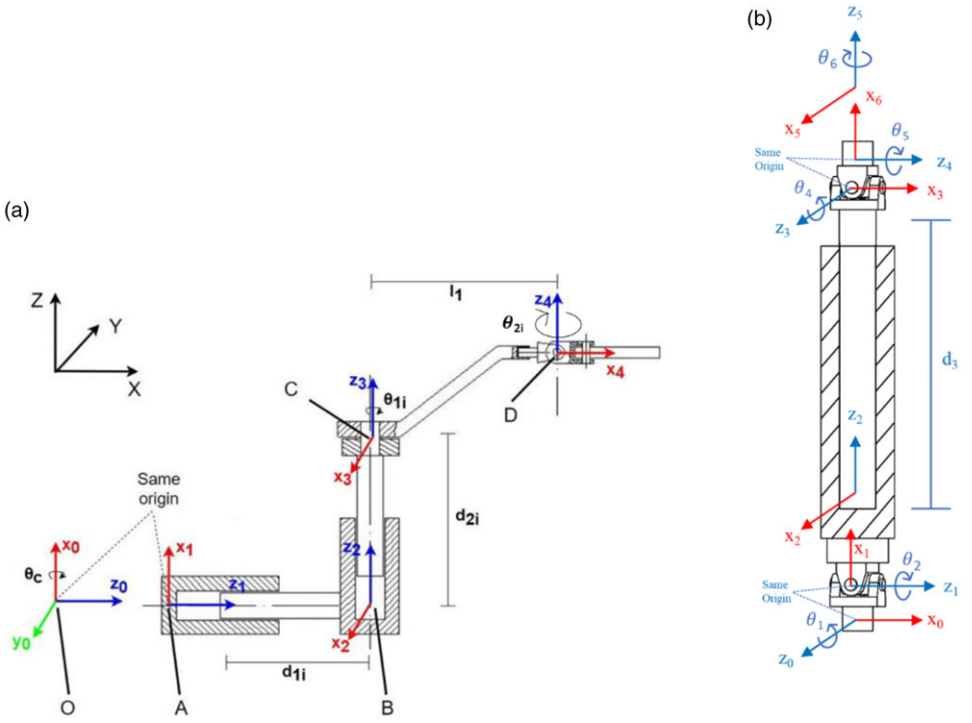

Figure 4. *Frame assignment for (a) a single leg and (b) passive load-balancing UPS leg.*

Table I. *D-H table for passive UPS leg of the 3-PPRS manipulator.*

D-H parameters	$\boldsymbol{\theta}$	$\boldsymbol{d}$	$\boldsymbol{\alpha}$	$\boldsymbol{a}$
${}^{0}T_{1}$	$\theta_1 + 90$	0	90	0
${}^{1}T_{2}$	$\theta_2 + 90$	0	90	0
${}^{2}T_{3}$	90	d_3	90	0
${}^{3}T_{4}$	$\theta_4 + 90$	0	90	0
${}^{4}T_{5}$	$\theta_5 + 90$	0	90	0
${}^{5}T_{6}$	θ_6	0	0	0

2. D-H methodology

In this section, the inverse kinematics is solved using the D-H methodology. The geometric description of the single leg and a UPS leg is shown in Fig. 4a. The d_{1i} and d_{2i} are the displacements of the linear actuators, and l_1 is the link length of the transmission link. θ_{1i} and θ_{2i} are the angle of rotational joints C and D, respectively.

The frame assignment for the passive load-balancing UPS leg is shown in Fig. 4b. The first universal joint is assigned with frame 0 and frame 1, followed by the prismatic joint assigned with frame 2, followed by the second universal joint, which is assigned with frames 3 and 4. The final frame 5 is assigned to the mobile platform. There are five joints serially connected, starting from two rotational joints with the same origin, then a prismatic joint and two rotational joints with the same origin. The respective joint axes x_n and z_n, are assigned to the joints. The angle for the rotational joint is θ_n, and the displacement for the linear joint is d_n. The D-H link and joint parameters are listed in Table I.

https://doi.org/10.1017/S0263574723000632 Published online by Cambridge University Press

The following equation gives the basic link transformation matrix,

$$^{i-1}T_i = \begin{bmatrix} C\theta_i & -S\theta_i C\alpha_i & S\theta_i S\alpha_i & a_i C\theta_i \\ S\theta_i & C\theta_i C\alpha_i & -C\theta_i S\alpha_i & a_i S\theta_i \\ 0 & S\alpha_i & C\alpha_i & d_i \\ 0 & 0 & 0 & 1 \end{bmatrix} \tag{1}$$

The D-H transformation matrices are derived by substituting the D-H parameters in the fundamental link transformation matrix. The D-H transformation matrices are as follows:

$$^0T_3 = {}^0T_2 \times {}^2T_3 = \begin{bmatrix} C\theta_1 & -S\theta_1 C\theta_2 & S\theta_1 S\theta_2 & -S\theta_1 C\theta_2 d_3 \\ S\theta_1 & C\theta_1 C\theta_2 & -C\theta_1 S\theta_2 & C\theta_1 C\theta_2 d_3 \\ 0 & S\theta_2 & C\theta_2 & S\theta_2 d_3 \\ 0 & 0 & 0 & 1 \end{bmatrix} \tag{2}$$

The stiffness analysis was carried out on the manipulator in its home position, with the mobile platform at zero orientation. In other words, without any tilt. As a result, the θ_4; θ_5; and θ_6 influences on end-effector orientation were considered to be zero.

$$^0T_6 = {}^0T_3 \times {}^3T_6 = \begin{bmatrix} S\theta_1 S\theta_2 & C\theta_1 & -S\theta_1 C\theta_2 & -S\theta_1 C\theta_2 d_3 \\ -C\theta_1 S\theta_2 & S\theta_1 & C\theta_1 C\theta_2 & C\theta_1 C\theta_2 d_3 \\ C\theta_2 & 0 & S\theta_2 & S\theta_2 d_3 \\ 0 & 0 & 0 & 1 \end{bmatrix} \tag{3}$$

The directions of the joint axes, P_{i-1}, derived using the equation $P_{i-1} = {}^0R_{i-1} \begin{bmatrix} 0 \\ 0 \\ 1 \end{bmatrix}$, are as follows:

The rotation matrix,

$$^0R_0 = \begin{bmatrix} 1 & 0 & 0 \\ 0 & 1 & 0 \\ 0 & 0 & 1 \end{bmatrix}; P_0 = {}^0R_0\widehat{u} = {}^0R_0 \begin{bmatrix} 0 \\ 0 \\ 1 \end{bmatrix} = \begin{bmatrix} 0 \\ 0 \\ 1 \end{bmatrix}; \tag{4}$$

$$^0R_1 = \begin{bmatrix} -S\theta_1 & 0 & C\theta_1 \\ C\theta_1 & 0 & S\theta_1 \\ 0 & 1 & 0 \end{bmatrix}; P_1 = {}^0R_1\widehat{u} = {}^0R_1 \begin{bmatrix} 0 \\ 0 \\ 1 \end{bmatrix} = \begin{bmatrix} C\theta_1 \\ S\theta_1 \\ 0 \end{bmatrix}; \tag{5}$$

$$^0R_2 = \begin{bmatrix} S\theta_1 S\theta_2 & C\theta_1 & -S\theta_1 C\theta_2 \\ -C\theta_1 S\theta_2 & S\theta_1 & C\theta_1 C\theta_2 \\ C\theta_2 & 0 & S\theta_2 \end{bmatrix}; P_2 = {}^0R_2\widehat{u} = {}^0R_2 \begin{bmatrix} 0 \\ 0 \\ 1 \end{bmatrix} = \begin{bmatrix} -S\theta_1 C\theta_2 \\ C\theta_1 C\theta_2 \\ S\theta_2 \end{bmatrix}; \tag{6}$$

$$^0R_3 = \begin{bmatrix} C\theta_1 & -S\theta_1 C\theta_2 & S\theta_1 S\theta_2 \\ S\theta_1 & C\theta_1 C\theta_2 & -C\theta_1 S\theta_2 \\ 0 & S\theta_2 & C\theta_2 \end{bmatrix}; P_3 = {}^0R_3\widehat{u} = {}^0R_3 \begin{bmatrix} 0 \\ 0 \\ 1 \end{bmatrix} = \begin{bmatrix} S\theta_1 S\theta_2 \\ -C\theta_1 S\theta_2 \\ C\theta_2 \end{bmatrix}; \tag{7}$$

$$^0R_4 = \begin{bmatrix} -S\theta_1 C\theta_2 & S\theta_1 S\theta_2 & C\theta_1 \\ C\theta_1 C\theta_2 & -C\theta_1 S\theta_2 & S\theta_1 \\ S\theta_2 & C\theta_2 & 0 \end{bmatrix}; P_4 = {}^0R_4\widehat{u} = {}^0R_4 \begin{bmatrix} 0 \\ 0 \\ 1 \end{bmatrix} = \begin{bmatrix} C\theta_1 \\ S\theta_1 \\ 0 \end{bmatrix}; \tag{8}$$

$$^0R_5 = \begin{bmatrix} S\theta_1 S\theta_2 & C\theta_1 & -S\theta_1 C\theta_2 \\ -C\theta_1 S\theta_2 & S\theta_1 & C\theta_1 C\theta_2 \\ C\theta_2 & 0 & S\theta_2 \end{bmatrix}; P_5 = {}^0R_5\widehat{u} = {}^0R_5 \begin{bmatrix} 0 \\ 0 \\ 1 \end{bmatrix} = \begin{bmatrix} -S\theta_1 C\theta_2 \\ C\theta_1 C\theta_2 \\ S\theta_2 \end{bmatrix}; \tag{9}$$

https://doi.org/10.1017/S0263574723000632 Published online by Cambridge University Press

The position vectors ${}^{i-1}P_6$, derived by applying the equation, ${}^{n}P_i = {}^{0}T_i O_i - {}^{0}T_n O_i$, are listed below

$$ {}^{0}P_6 = {}^{0}T_6 O_6 - {}^{0}T_0 O_6 = \begin{bmatrix} -S\theta_1 C\theta_2 d_3 \\ C\theta_1 C\theta_2 d_3 \\ S\theta_2 d_3 \\ 1 \end{bmatrix} - \begin{bmatrix} 0 \\ 0 \\ 0 \\ 1 \end{bmatrix} = \begin{bmatrix} -S\theta_1 C\theta_2 d_3 \\ C\theta_1 C\theta_2 d_3 \\ S\theta_2 d_3 \\ 0 \end{bmatrix}; \tag{10} $$

$$ {}^{1}P_6 = {}^{0}T_6 O_6 - {}^{0}T_1 O_6 = \begin{bmatrix} -S\theta_1 C\theta_2 d_3 \\ C\theta_1 C\theta_2 d_3 \\ S\theta_2 d_3 \\ 1 \end{bmatrix} - \begin{bmatrix} 0 \\ 0 \\ 0 \\ 1 \end{bmatrix} = \begin{bmatrix} -S\theta_1 C\theta_2 d_3 \\ C\theta_1 C\theta_2 d_3 \\ S\theta_2 d_3 \\ 0 \end{bmatrix}; \tag{11} $$

The Jacobian matrix does not require the position vector ${}^{2}P_6$. Because it corresponds to the prismatic joint, only the direction of the joint axis P_2 is required.

Also,

$$ {}^{3}P_6 = {}^{4}P_6 = {}^{5}P_6 = \begin{bmatrix} 0 \\ 0 \\ 0 \end{bmatrix}; \tag{12} $$

3. Stiffness analysis using Jacobian matrix

The Jacobian matrix for a manipulator with non-planar links is obtained using the screw theory principle. The input/actuator velocities are transformed to the end-effector output velocity using a Jacobian velocity matrix. The Jacobian matrix can also be used to find singular configurations of the manipulator in which it gains one or more DOF.

The end-effector's twist is related to the joint rate vector $\dot{\boldsymbol{\theta}}$ by

$$ J\dot{\boldsymbol{\theta}} = t \tag{13} $$

$$ \dot{\boldsymbol{\theta}} = \begin{bmatrix} \dot{d}_{1i} & \dot{d}_{2i} & \dot{\theta}_{1i} & \dot{\theta}_{4i} & \dot{\theta}_{5i} & \dot{\theta}_{6i} \end{bmatrix}^T ; i\text{denotes leg } i, t = \begin{bmatrix} \omega \\ \dot{c} \end{bmatrix} \tag{14} $$

where J is the screw-based velocity Jacobian matrix for UPS configuration

$$ J = \begin{bmatrix} P_0 \times {}^{0}P_6 & P_1 \times {}^{1}P_6 & P_2 & P_3 \times {}^{3}P_6 & P_4 \times {}^{4}P_6 & P_5 \times {}^{5}P_6 \\ P_0 & P_1 & 0 & P_3 & P_4 & P_5 \end{bmatrix} \tag{15} $$

P_i is the joint i's direction vector. ${}^{n}P_i$ is the position vector pointing from the i^{th} joint to the end-effector. The values of position vectors and the direction of joint axes are imported from Section 2 for Jacobian calculations.

For the 1st joint (revolute),

$$ J_1 = \begin{bmatrix} P_0 \times {}^{0}P_6 \\ P_0 \end{bmatrix} \tag{16} $$

$$ J_1 = \begin{bmatrix} \begin{bmatrix} 0 \\ 0 \\ 1 \end{bmatrix} \times \begin{bmatrix} -S\theta_1 C\theta_2 d_3 \\ C\theta_1 C\theta_2 d_3 \\ S\theta_2 d_3 \end{bmatrix} \\ \begin{bmatrix} 0 \\ 0 \\ 1 \end{bmatrix} \end{bmatrix} = \begin{bmatrix} -C\theta_1 C\theta_2 d_3 \\ -S\theta_1 C\theta_2 d_3 \\ 0 \\ 0 \\ 0 \\ 1 \end{bmatrix} \tag{17} $$

https://doi.org/10.1017/S0263574723000632 Published online by Cambridge University Press

The 3rd joint (prismatic),

$$J_i = \begin{bmatrix} P_{i-1} \\ 0 \end{bmatrix}; J_3 = \begin{bmatrix} -S\theta_1 C\theta_2 \\ C\theta_1 C\theta_2 \\ S\theta_2 \\ 0 \\ 0 \\ 0 \end{bmatrix} \tag{18}$$

Similarly, the Jacobian for the other joints J_4, J_5, and J_6 is computed.

$$J_2 = \begin{bmatrix} S\theta_1 S\theta_2 d_3 \\ -C\theta_1 S\theta_2 d_3 \\ C\theta_2 d_3 \\ C\theta_1 \\ S\theta_1 \\ 0 \end{bmatrix} J_4 = \begin{bmatrix} 0 \\ 0 \\ 0 \\ S\theta_1 S\theta_2 \\ -C\theta_1 S\theta_2 \\ C\theta_2 \end{bmatrix}; J_5 = \begin{bmatrix} 0 \\ 0 \\ 0 \\ C\theta_1 \\ S\theta_1 \\ 0 \end{bmatrix}; J_6 = \begin{bmatrix} 0 \\ 0 \\ 0 \\ -S\theta_1 C\theta_2 \\ C\theta_1 C\theta_2 \\ S\theta_2 \end{bmatrix} \tag{19}$$

The Jacobian matrix for the UPS configuration is given below, $J = \begin{bmatrix} J_1 & J_2 & J_3 & J_4 & J_5 & J_6 \end{bmatrix}$

$$J_{UPS} = \begin{bmatrix} -C\theta_1 C\theta_2 d_3 & S\theta_1 S\theta_2 d_3 & -S\theta_1 C\theta_2 & 0 & 0 & 0 \\ -S\theta_1 C\theta_2 d_3 & -C\theta_1 S\theta_2 d_3 & C\theta_1 C\theta_2 & 0 & 0 & 0 \\ 0 & C\theta_2 d_3 & S\theta_2 & 0 & 0 & 0 \\ 0 & C\theta_1 & 0 & S\theta_1 S\theta_2 & C\theta_1 & -S\theta_1 C\theta_2 \\ 0 & S\theta_1 & 0 & -C\theta_1 S\theta_2 & S\theta_1 & C\theta_1 C\theta_2 \\ 1 & 0 & 0 & C\theta_2 & 0 & S\theta_2 \end{bmatrix} \tag{20}$$

3.1. Stiffness map results

The parallel manipulator configuration proposed in this article comprises two main components: the constraining leg, which can be considered a serial (passive), and the 3-PPRS manipulator as a parallel (active) mechanism. As a result, the overall stiffness matrix of the parallel mechanism with a constraining leg can be obtained by adding the stiffness matrices of the parallel and serial mechanisms [20]. The stiffness matrix for the manipulator, including the UPS constraining leg, is given by,

$$K = K_{UPS} + K_{parallel}; \tag{21}$$

where

$$K_{UPS} = \left(J'_{UPS}\right)^{-T} K_{dia} \left(J'_{UPS}\right)^{-1} \tag{22}$$

By the principle of the virtual joint method [21], the diagonal stiffness matrix K_{dia} is given as follows:

$$K_{dia} = diag\,[0, K_6, 0, 0, 0, 0] \tag{23}$$

Within the workspace, the stiffness of the UPS leg K_{UPS} in the X-Y plane is determined. The D-H methodology discussed in Section 2 is used to solve the inverse kinematics of the UPS configuration. With the solved UPS parameters (joint angles and displacement), the Jacobian $J_{UPS}$is computed, and hence the stiffness of the UPS leg.

As the spatial motion actuators of the 3-PPRS manipulator are aligned along Z axis, the configuration has high torsional stiffness. Hence, the translational stiffness alone is studied. The stiffness values Kx and Kz in the X-Y plane are plotted in Fig. 5. The stiffness values Kx are high around the region of the home position, and the values are five times larger compared to Kz values. The stiffness in X-axis is a valuable addition to this parallel manipulator (3-PPRS) because the existing parallel manipulator has one of the planar motion actuators aligned along the X-axis. Including UPS leg in the 3-PPRS parallel manipulator will enhance its translational stiffness.

https://doi.org/10.1017/S0263574723000632 Published online by Cambridge University Press

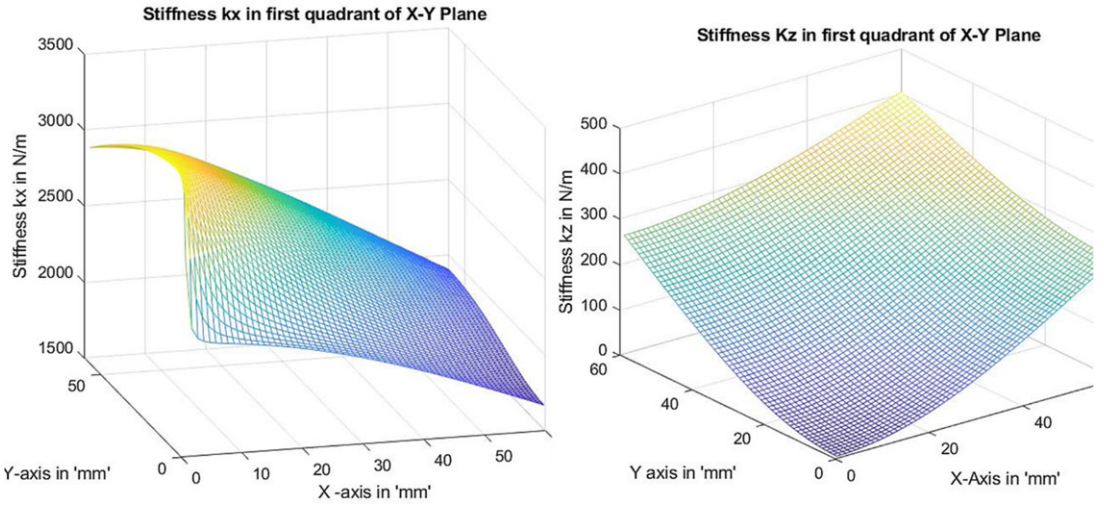

Figure 5. *Stiffness plot for Kx and Kz in the X-Y plane for the UPS configuration.*

4. Static structural analysis of 3-PPRS parallel manipulator

Using ANSYS Workbench software, the structural analysis of the three different 3-PPRS parallel manipulator architectures, namely the 3-PPRS manipulator with planar transmission links, the 3-PPRS manipulator with spatial transmission links, and the 3-PPRS manipulator with spatial transmission links in addition to the passive load-balancing UPS leg, is compared. In this article, the load balancing of the entire manipulator is of prime interest. The vertical hydraulic actuators predominantly carrying the load against gravity are only considered for static structural analysis. On the other hand, the horizontal electrical actuators not carrying any load against gravity are excluded from the analysis, simplifying the computer-aided design (CAD) model.

Three architectures are structurally compared in the static structural analysis [22] using total deformation and equivalent stress (Von Mises). In the ANSYS Workbench Static Structural tool, the CAD models of the 3-PPRS manipulator are imported from SolidWorks as step files, and the manipulator's material was set to mild steel (MS). The fixed platform is fastened to the ground, and a load of 5000 N is applied to the center of the mobile platform. The results of the static structural simulation are shown in Figs. 6–7.

4.1. Results of structural analysis

From Tables II-III, it is clear that compared to the other two 3-PPRS manipulator architectures, the one with both spatial transmission links and a passive load balancing leg has the least total deformation value (0.02581 mm) and the lowest Von Mises equivalent stress (72.30 MPa). The proposed architecture is designed safe because the selected material (MS) has a tensile yield strength of 250 MPa [23]. Thus, the architecture of a 3-PPRS manipulator with spatial transmission links and a passive load-balancing UPS leg is determined to be effective based on the analytical results and selected for manufacturing.

5. Dynamic system modeling

Due to the manipulator assembly's symmetrical nature, a single-leg assembly model is considered [24]. The specimen model includes the model of the transmission link, push rod, and specimen. Hence, the stiffness of the link, push rod, and specimen are added, as shown in Fig. 8. Specimen stiffness indicates the stiffness of the specimen, connecting link, and the pushrod, and it is represented as K_{sp}. Similar is the case with specimen damping C_{sp}. The oil column in the cylinder is compressible, and it is represented by a stiffness of K_a and damping of C_a.

https://doi.org/10.1017/S0263574723000632 Published online by Cambridge University Press

(a)

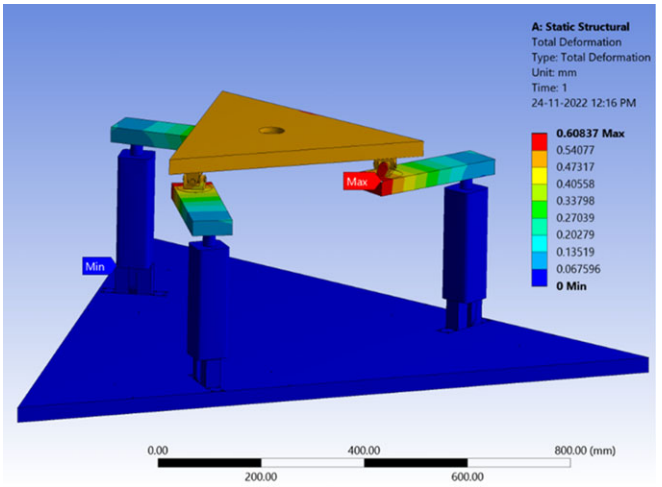

planar transmission links

(b)

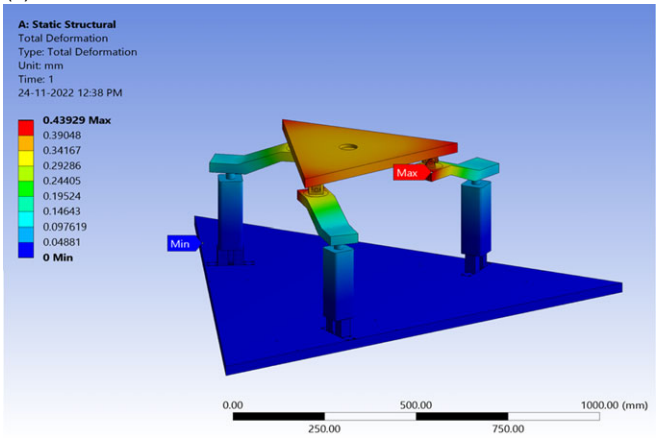

spatial transmission links

(c)

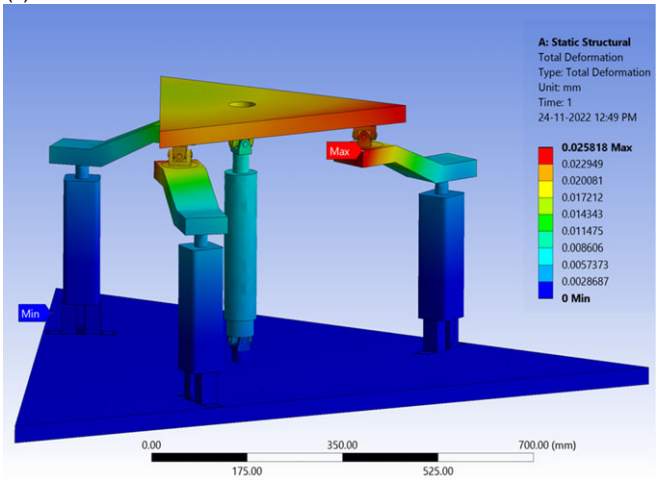

combination of spatial transmission links and a passive UPS load-balancing leg

Figure 6. *The total deformation for the three different architectures of the 3-PPRS manipulator.*

https://doi.org/10.1017/S0263574723000632 Published online by Cambridge University Press

(a)

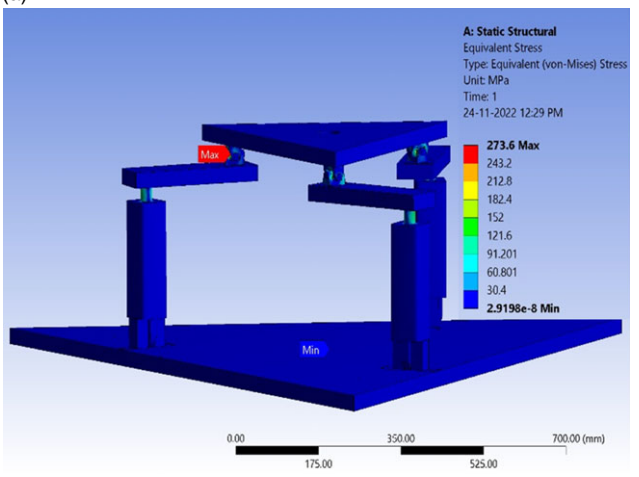

planar transmission links

(b)

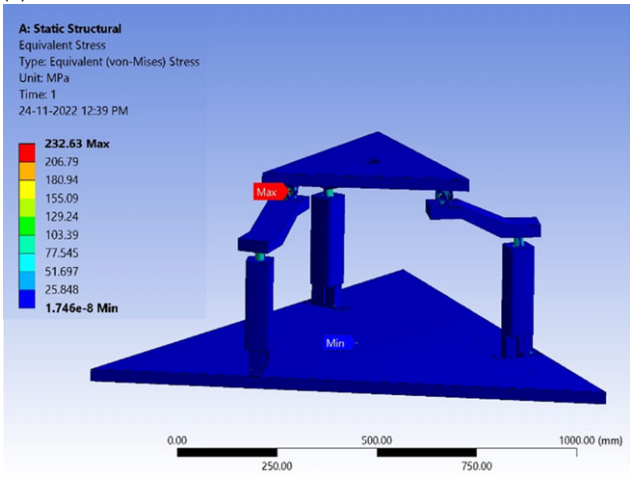

spatial transmission links

(c)

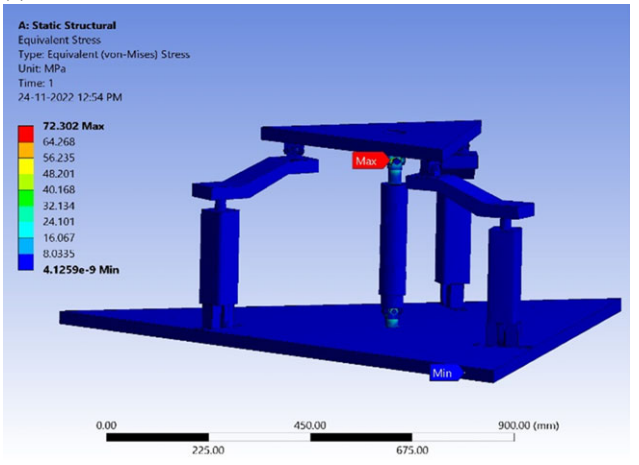

a combination of spatial transmission links and a passive UPS load-balancing leg

Figure 7. *The equivalent stress for three different architectures of the 3-PPRS manipulator.*

https://doi.org/10.1017/S0263574723000632 Published online by Cambridge University Press

Table II. *Total deformation of the 3-PPRS manipulator.*

Architecture: 3-PPRS	Minimum[mm]	Maximum[mm]
With planar links	0	0.608
With spatial links	0	0.439
With spatial links and UPS leg	0	0.026

Table III. *Equivalent stress of 3-PPRS manipulator.*

Architecture: 3-PPRS	Minimum [MPa]	Maximum [MPa]
With planar links	2.92×10^{-8}	273.60
With spatial links	1.75×10^{-8}	232.63
With spatial links and UPS leg	4.12×10^{-9}	72.30

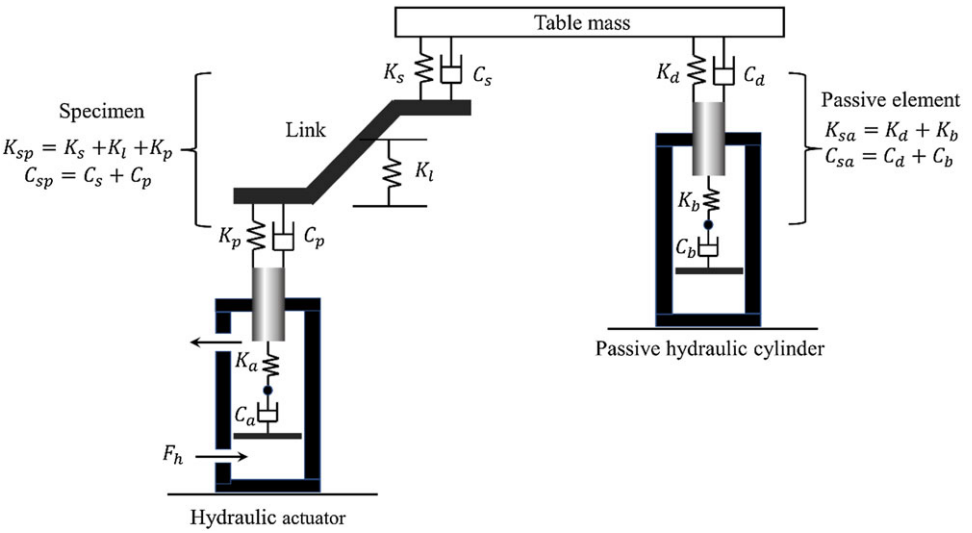

Figure 8. *The mechanical model of a single actuator leg and a passive hydraulic cylinder.*

The UPS leg is modeled as a passive hydraulic cylinder in Case 1 and a passive damper in Case 2. In the case of a passive damper, it is modeled as a non-linear spring. It means the spring force will be larger at the compressed state and minimum at the extended state [25]. The spring force is proportional to the displacement by the passive damper, which will be the difference between the total spring length and actual displacement, that is, $(z_{max} - z_t)$. The mass is considered negligible because of its passive nature.

5.1. Case 1 modeling of UPS leg as a passive hydraulic cylinder

The mechanical model of the single actuator leg and the UPS leg as a passive hydraulic cylinder is shown in Fig. 8. The passive hydraulic cylinder contains a linear spring (K_b) and damper (C_b).

The free-body diagram of the above mechanical model is shown in Fig. 9.

Upward direction is the positive sign convention for displacements z_p and z_t. Summing all external forces with an upward direction as the positive sign convention and applying Newton's second law, for

$$\text{Mass } (M_p){:}+\uparrow \sum F = -K_{sp}(z_p - z_t) - C_{sp}(\dot{z_p} - \dot{z_t}) - K_a z_p - C_a \dot{z_p} + F_h = M_p \ddot{z_p} \tag{24}$$

$$\text{Mass } (M_t){:}+\uparrow \sum F = K_{sp}(z_p - z_t) + C_{sp}(\dot{z_p} - \dot{z_t}) - K_{sa} z_t - C_{sa} \dot{z_t} = M_t \ddot{z_t} \tag{25}$$

https://doi.org/10.1017/S0263574723000632 Published online by Cambridge University Press

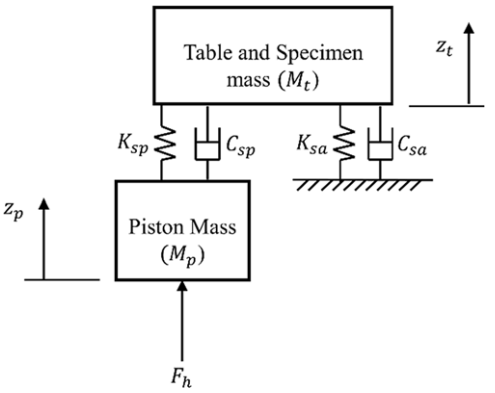

Figure 9. *The free-body diagram of the mechanical model with UPS leg as a passive hydraulic cylinder.*

Rearranging these equations with dynamic variables (z_p and z_t) on the left-hand side and the input variable F_h on the right-hand side,

$$M_p\ddot{z_p} + C_{sp}\left(\dot{z_p} - \dot{z_t}\right) + K_{sp}\left(z_p - z_t\right) + K_a z_p + C_a\dot{z_p} = F_h \tag{26}$$

$$M_t\ddot{z_t} + C_{sp}\left(\dot{z_t} - \dot{z_p}\right) + K_{sp}\left(z_t - z_p\right) + K_{sa}z_t + C_{sa}\dot{z_t} = 0 \tag{27}$$

Equations (26) and (27) represent the mathematical model of the single actuator leg and the load-balancing UPS leg. As there are two inertia elements, $M_t\&M_p$, the model consists of two second-order ordinary differential equations (ODEs). Since both ODEs are coupled, solving one ODE separately from the other is impossible. In Case 1, the model is linear because we have assumed linear stiffness and damper elements. In general, this condition is suitable for an inherently stable system. Intuition tells us that the shake table model is stable and will always return to static equilibrium when input hydraulic force F_h is stopped.

Writing equation (27) in the Laplace form,

$$M_t s^2 z_t + C_{sp}s\left(z_t - z_p\right) + K_{sp}\left(z_t - z_p\right) + K_{sa}z_t + C_{sa}sz_t = 0 \tag{28}$$

$$z_t\left(M_t s^2 + C_{sp}s + K_{sp} + K_{sa} + C_{sa}s\right) = -z_p\left(-C_{sp}s - K_{sp}\right) \tag{29}$$

By rearranging the above equation, the relation between pushrod displacement and table displacement is obtained in equation (30),

$$\frac{z_t}{z_p} = \frac{C_{sp}s + K_{sp}}{\left(M_t s^2 + \left(C_{sp} + C_{sa}\right)s + \left(K_{sp} + K_{sa}\right)\right)} \tag{30}$$

Writing equation (26) in the Laplace form,

$$M_p s^2 z_p + C_{sp}s\left(z_p - z_t\right) + K_{sp}\left(z_p - z_t\right) + K_a z_p + C_a s z_p = F_h \tag{31}$$

$$z_p\left(M_p s^2 + C_{sp}s + K_{sp} + C_a s + K_a\right) + z_t\left(-C_{sp}s - K_{sp}\right) = F_h \tag{32}$$

$$z_p = \frac{z_t\left(C_{sp}s + K_{sp}\right) + F_h}{M_p s^2 + \left(C_{sp} + C_a\right)s + \left(K_{sp} + K_a\right)} \tag{33}$$

Substituting z_p value in equation (30), and upon simplification, the following relations between displacements z_t & z_p and the hydraulic force (F_h) applied to the piston are obtained

$$\frac{z_t}{F_h} = \frac{A'}{\left(M_p s^2 + C'\right)B' - A'^2} \tag{34}$$

https://doi.org/10.1017/S0263574723000632 Published online by Cambridge University Press

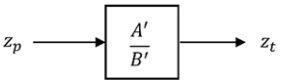

Figure 10. *The conceptual realization of the passive hydraulic cylinder transfer function is shown in equation (30).*

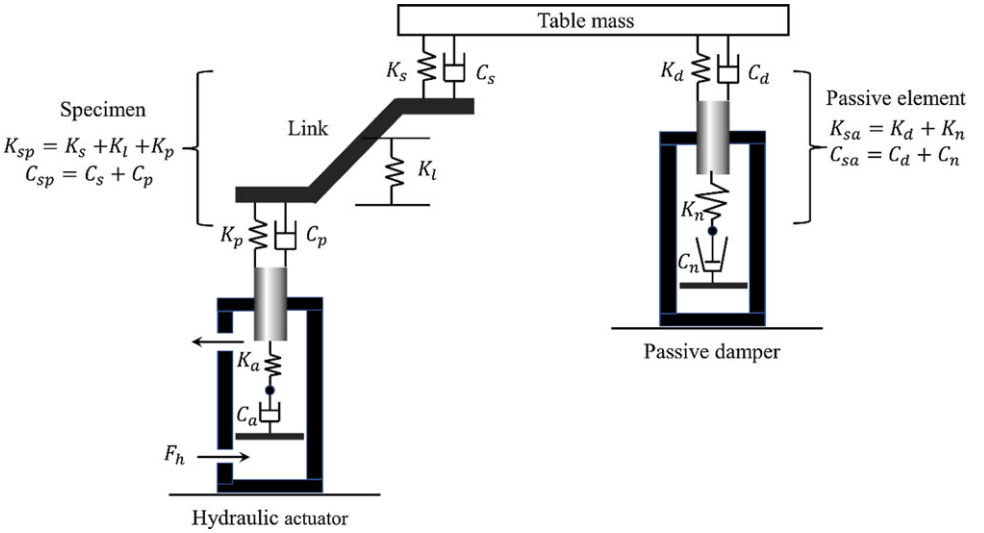

Figure 11. *The mechanical model of a single actuator leg and a passive hydraulic damper.*

Similarly,

$$\frac{z_p}{F_h} = \frac{B'}{\left(M_p s^2 + C'\right) B' - A'^2} \tag{35}$$

where

$$A' = C_{sp} s + K_{sp} \tag{36}$$

$$B' = M_t s^2 + \left(C_{sp} + C_{sa}\right) s + \left(K_{sp} + K_{sa}\right) \tag{37}$$

$$C' = \left(C_{sp} + C_a\right) s + \left(K_{sp} + K_a\right) \tag{38}$$

The graphical representation of equation (30) is shown in Fig. 10.

5.2. Case 2 modeling of UPS leg as a passive damper

The mechanical model of the single actuator leg and the UPS leg as a passive damper is shown in Fig. 11. The passive damper contains the non-linear spring (K_n) and damper (C_n). The non-linear spring and damper are differentiated structurally from linear spring and damper, as shown in Fig. 11.

The free-body diagram of the above mechanical model is given in Fig. 12. The initially compressed spring and damper of the passive damper element are indicated in the free-body diagram by blue dotted lines. The displacement offered by the passive damper will be $(z_{max} - z_t)$. Since stroke length is constant $(\dot{z_{max}} = 0)$.

Equation (27) becomes

$$M_t \ddot{z_t} + C_{sp}\left(\dot{z_t} - \dot{z_p}\right) + K_{sp}\left(z_t - z_p\right) - K_{sa}\left(z_{max} - z_t\right) - C_{sa}\left(\dot{z_{max}} - \dot{z_t}\right) = 0 \tag{39}$$

https://doi.org/10.1017/S0263574723000632 Published online by Cambridge University Press

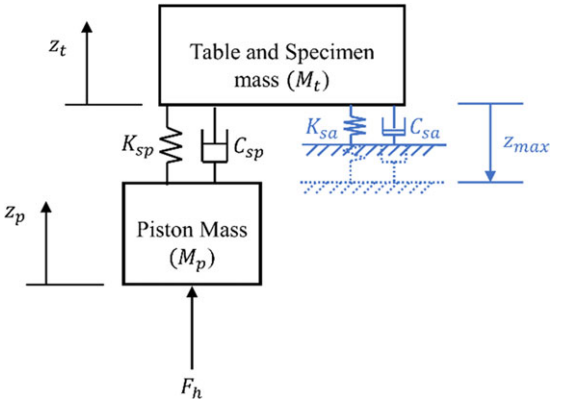

Figure 12. *The free-body diagram of the mechanical model with UPS leg as a passive damper.*

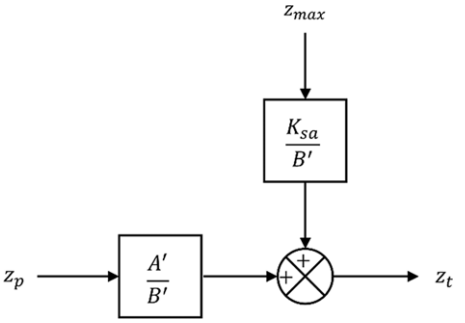

Figure 13. *The conceptual realization of the passive damper model transfer function is shown in equation (43).*

Writing the above equation in the Laplace form,

$$M_t s^2 z_t + C_{sp} s\left(z_t - z_p\right) + K_{sp}\left(z_t - z_p\right) - K_{sa} z_{max} + K_{sa} z_t + C_{sa} s z_t = 0 \tag{40}$$

$$z_t\left(M_t s^2 + \left(C_{sp} + C_{sa}\right) s + K_{sp} + K_{sa}\right) - K_{sa} z_{max} = z_P\left(C_{sp} s + K_{sp}\right) \tag{41}$$

On further simplification, the relation between the table displacement (z_t) and the pushrod displacement (z_P) is obtained in equation (43).

$$z_t B' = z_P A' + K_{sa} z_{max} \tag{42}$$

$$z_t = z_P \frac{A'}{B'} + \frac{K_{sa} z_{max}}{B'} \tag{43}$$

The inclusion of a passive damper causes an additional term in the transfer function model, $K_{sa} z_{max}$, which appears to be a disturbance in equation 42. The passive damper element comprises a non-linear spring [26] which is initially compressed to provide high spring force. This nonlinearity in the model provides force compensation during the upward displacement of the mobile platform z_t (load against gravity) which was captured as DC gain in Fig. 17.

The graphical representation of equation (43) is shown in Fig. 13.

5.3. Stability results and damping analysis

The following sections present the stability results and damping analysis for Cases 1 and 2.

https://doi.org/10.1017/S0263574723000632 Published online by Cambridge University Press

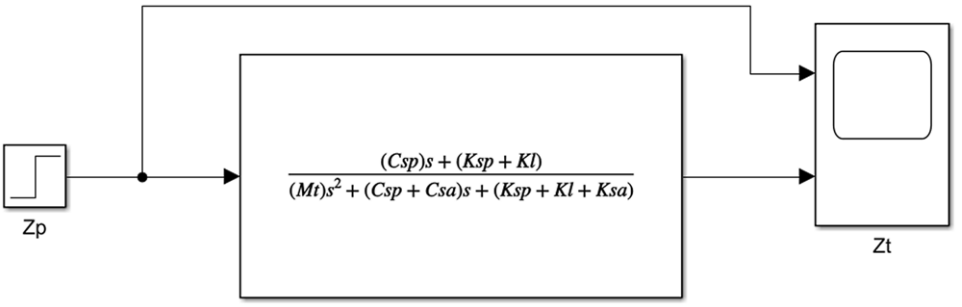

Figure 14. *The Simulink transfer function model for the passive cylinder.*

Table IV. *The parameter values for the transfer functions.*

Parameter	Value
C_{sp}	3×10^5Ns/m
C_{sa}	3.18×10^6Ns/m
K_l	2×10^6N/m
K_{sp}	5×10^8N/m
K_{sa}	5×10^7N/m
M_t	2700 Kg

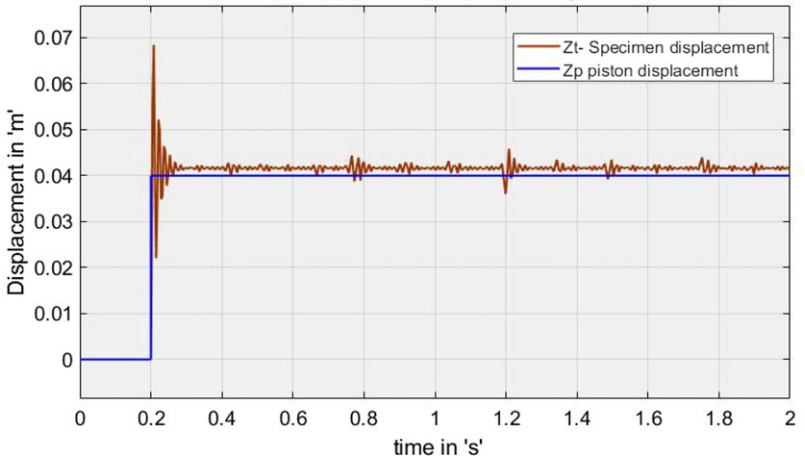

Figure 15. *The response plot of the passive hydraulic cylinder.*

5.3.1. For Case 1: passive hydraulic cylinder

From equation (30), it can be inferred that K_{sa} appears on the denominator of the transfer function. Hence, the value of K_{sa} should be chosen 0.1 times the value of K_{sp}. This will ensure that the DC gain remains unaffected. A step signal is given as input to the transfer function of the passive hydraulic cylinder given by equation (30). The Simulink model for the transfer function is displayed in Fig. 14.

The parameter values for the transfer functions are chosen from Table IV.

In the case of a passive hydraulic cylinder as the load-balancing UPS leg, the output displacement of the specimen/table shows overshoot and vibrations, as illustrated in Fig. 15.

As shown in Table V, the system is stable (since all the complex poles of the transfer function are in the left half of the s-plane), but it is underdamped (damping ratio $\zeta < 1$).

https://doi.org/10.1017/S0263574723000632 Published online by Cambridge University Press

Table V. *Transfer function parameter table for the passive hydraulic cylinder.*

Pole	Damping ratio	Frequency (rad/s)	Time constant (s)
−58.9 + 452i	0.129	456	0.017
−58.9 − 452i	0.129	456	0.017
−58.9 + 452i	0.129	456	0.017
−58.9 − 452i	0.129	456	0.017

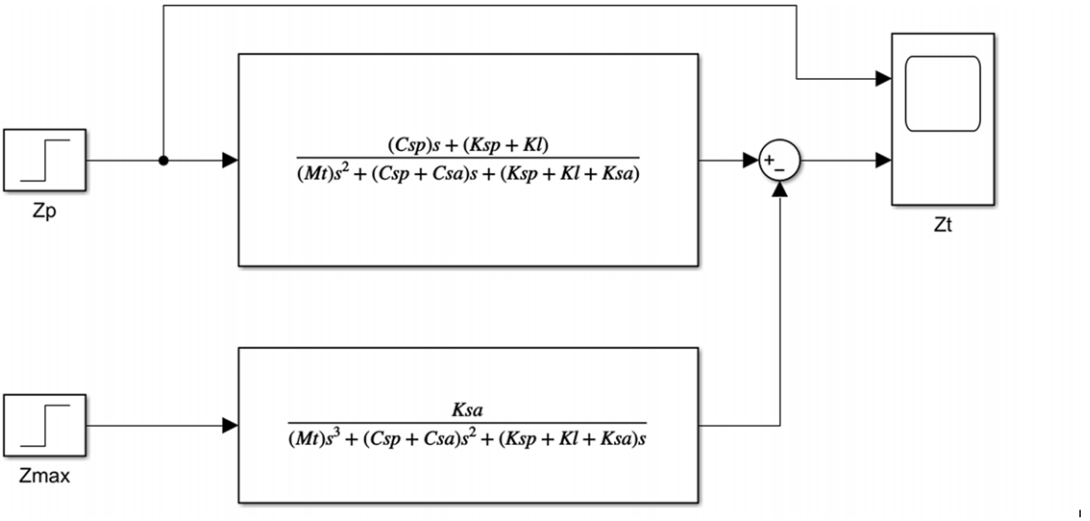

Figure 16. *The Simulink transfer function model for the passive damper.*

5.3.2. For Case 2: passive damper element

Equation (43) represents the transfer of the passive damper element. The K_{sa} value is $(K_n + K_b)$, where K_n represents the non-linear part of the damper (Fig. 11). After estimating the non-linear value of K_n, the K_{sa} value was determined to be 1×10^8 N/m. Similarly, the C_{sa} value is estimated to be 3.18×10^6 Ns/m (Table IV), which is ten times larger than C_{sp}. Due to this, the damping of the model improved, as shown in Fig. 17.

A step signal is given as input to the transfer function of the passive damper model given by equation (43). The Simulink model for the transfer function is displayed in Fig. 16.

With the inclusion of a passive hydraulic damper in the model, the vibrations are suppressed, and the DC gain factor increases, as shown in Fig. 17.

As shown in Table VI, the system is stable (the two complex poles and two real poles of the transfer function are in the left half of the s-plane) and critically damped (damping ratio $\zeta = 1$).

6. Conclusion

Including a passive damper element (a UPS leg) in the 3-PPRS parallel manipulator is proposed in this article, which addresses both the load balancing and force compensation issues common in parallel spatial manipulators. The UPS leg is analyzed using a passive hydraulic cylinder (linear) and a passive damper (non-linear). For the first time, such damper elements were introduced in the parallel manipulator, and its nonlinearity was captured in the detailed mathematical modeling. A comparative study was performed using standard balancing mechanisms such as a passive hydraulic cylinder.

The following specific conclusions can be drawn:

1. From the stiffness map results, adding a UPS-load balancing leg to the 3-PPRS parallel manipulator improves the overall stiffness of the load-bearing assembly.

https://doi.org/10.1017/S0263574723000632 Published online by Cambridge University Press

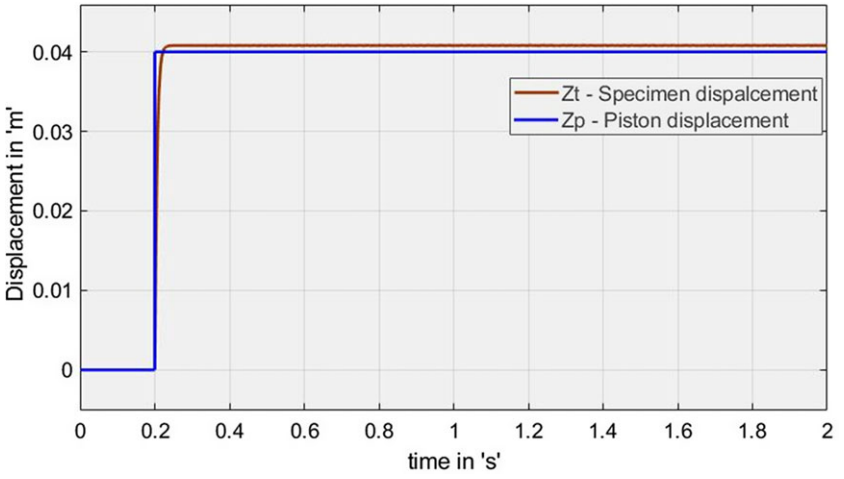

Figure 17. *The response plot of the passive damper model.*

Table VI. *Transfer function parameter table for passive damper model.*

Pole	Damping ratio	Frequency (rad/s)	Time constant (s)
$-195 + 6.27 \times 10^{-6}$ i	1	195	0.005
$-195 + 6.27 \times 10^{-6}$ i	1	195	0.005
-1100	1	1100	0.005
-1100	1	1100	0.005

2. The architecture of a 3-PPRS manipulator with spatial transmission links and a passive load-balancing UPS leg is effective in terms of total deformation and equivalent stress.
3. From the detailed dynamic system modeling, the inclusion of a passive damper to a 3-PPRS system is found to be stable and critically damped. This damping is highly desirable for applications such as seismic simulation and flight simulation. On the other hand, including a passive hydraulic cylinder in a 3-PPRS system is found to be stable but underdamped, which is undesirable.
4. The DC gain in the response indicates that the passive damper element aided the force compensation during the upward displacement of the mobile platform z_t (against gravity). For future study, the downward displacement of the mobile platform z_t will be considered.

As a result, the improved configuration of the 3-PPRS parallel manipulator with a passive damper proposed in this article is desirable for enhanced system stiffness and damping and force compensation for counteracting the load against gravity.

Acknowledgements. The authors express their gratitude to SASTRA Deemed to be University, Thanjavur, for the learning facility created and Rodyne Systems India Private Limited, Bangaluru for providing fabrication service.

Author contributions. **A. Xavier Reni Prasad:** Design and software analysis, preparing the manuscript.
M. Ganesh: Conceptualization, supervision, project administration, funding acquisition.

Financial support. The project was funded by DST-SERB, India, project no. ECR/2018/002443, to which the authors like to express their gratitude.

Competing interest declaration. The author(s) have no competing interests.

https://doi.org/10.1017/S0263574723000632 Published online by Cambridge University Press

References

[1] Y. Yilmaz and G. Anlas, "An investigation of the effect of counterweight configuration on main bearing load and crankshaft bending stress," *Adv. Eng. Softw.* **40**(2), 95–104 (2009).

[2] J. Woo, J. T. Seo and B. J. Yi, "A static balancing method for variable payloads by combination of a counterweight and spring and its application as a surgical platform," *Appl. Sci.* **9**(19), 1–21 (2019).

[3] F. Wildenberg, "Compensating System for a Hexapod, 2002, U.S. Patent No. 6,474,915,

[4] A. Martini, M. Troncossi, M. Carricato and A. Rivola, "Static balancing of a parallel kinematics machine with Linear-Delta architecture: Theory, design and numerical investigation," *Mech. Mach. Theory* **90**, 128–141 (2015).

[5] S. K. Agrawal and A. Fattah, "Gravity-balancing of spatial open-chain manipulators," *Mech. Mach. Theory* **39**(12), 1331–1344 (2004).

[6] C.-W. Juang, C.-S. Jhuang and D.-Z. Chen, "Spring-balanced 3-DoF serial planar manipulators for constant forces in arbitrary directions," *Robotica*, 1–19 (2023).

[7] M. Leblond and C. M. Gosselin. Static Balancing of Spatial and Planar Parallel Manipulators with Prismatic Actuators". **In:** Proceedings of DETC'98, Atlanta, GA (1998) pp. 1–12.

[8] I. Ebert-Uphoff, C. M. M. Gosselin and T. Laliberte', "Static balancing of spatial parallel platform mechanisms-revisited," *J. Mech. Design* **122**(1), 43–51 (2000).

[9] I. Ebert-Uphoff and K. Johnson, "Practical considerations for the static balancing of mechanisms of parallel architecture," *Proc. Inst. Mech. Eng. K J. Multi-body Dyn.* **216**(1), 73–85 (2002).

[10] V. A. Arakelian and S. Guegan, "Design and prototyping of a new balancing mechanism for spatial parallel manipulators," *J. Mech. Design*, (2008).

[11] J. Wang and X. Kong, "A geometric approach to the static balancing of mechanisms constructed using spherical kinematic chain units," *Mech. Mach. Theory* **140**, 305–320 (2019).

[12] B. Wei and D. Zhang, "A review of dynamic balancing for robotic mechanisms," *Robotica* **39**(1), 55–71 (2021).

[13] G. Mangavu and A. K. Dash, "Design, static analysis and development of a new three-legged shake table," *Proc. Inst. Mech. Eng. C: J. Mech. Eng. Sci.* **236**(3), 1571–1587 (2022).

[14] M. Ganesh, A. K. Dash, P. Venkitachalam and S. Shrinithi, "Static characteristic analysis of spatial (non-planar) links in planar parallel manipulator," *Robotica* **39**(1), 88–106 (2021).

[15] S. Ammanagi, V. Poornima, A. Sera and R. Sunder, "Development of a digitally-controlled three-axis earthquake shake table," *Curr. Sci.*, 190–203 (2006).

[16] M. Omar, M. M. El-kassaby and W. Abdelghaffar, "A universal suspension test rig for electrohydraulic active and passive automotive suspension system," *Alexandria Eng. J.* **56**(4), 359–370 (2017).

[17] Y. Lu and B. Hu, "Unified solving Jacobian/Hessian matrices of some parallel manipulators with n SPS active legs and a passive constrained leg," *J. Mech. Design* **129**(11), 1161–1169 (2007).

[18] J. Wang and C. M. Gosselin, "Static balancing of spatial four-degree-of-freedom parallel mechanisms," *Mech. Mach. Theory* **35**(4), 563–592 (2000).

[19] J. Zhang, Y. Zhao and Y. Jin, "Kinetostatic-model-based stiffness analysis of Exechon PKM," *Robot. Comput. Integr. Manuf.* **37**, 208–220 (2016).

[20] D. Zhang and C. M. M. Gosselin, "Kinetostatic modeling of N-DOF parallel mechanisms with a passive constraining leg and prismatic actuators," *J. Mech. Design* **123**(3), 375–381 (2001).

[21] A. Pashkevich, A. Klimchik and D. Chablat, "Enhanced stiffness modeling of manipulators with passive joints," *Mech. Mach. Theory* **46**(5), 662–679 (2011).

[22] H. Zhang, J. Tang, C. Yan, G. Cui, M. Zhang and Y. Yao, "Stiffness analysis of a 3-DOF parallel mechanism for engineering special machining," *Mech. Sci.* **13**(2), 635–645 (2022).

[23] R. Jha, S. Ranjan, R. Kumar, M. Sharma and R. Scholar, "Investigation of heat treatment on mechanical properties of mild steel," *An. Int. J. Eng. Sci.* **25**(63019), 2320–0332 (2017).

[24] A. R. Plummer, "A detailed dynamic model of a six-axis shaking table," *J. Earthq. Eng* **12**(4), 631–662 (2008).

[25] C. A. Kluever, "Craig A. Kluever - Dynamic Systems: Modeling, Simulation, and Control," Wiley, (2015) pp. 488,

[26] B. Abebe, J. Santhosh, A. A. Ahmed and M. Ponnusamy, "Non-linear mathematical modelling for quarter car suspension model," *Int. J. Emerg. Technol.* **11**(5), 536–544 (2020).

https://doi.org/10.1017/S0263574723000632 Published online by Cambridge University Press

Appendix: Symbols and Notations

C_a	Internal cylinder damping
C_b	Internal damping of passive cylinder or damper
C_d	Piston damping of passive cylinder or damper
C_p	Pushrod damping of the hydraulic actuator
C_s	Damping of table and specimen
C_{sa}	Damping of UPS leg
C_{sp}	Specimen damping
d_n	Displacement of the linear joint
F_h	The hydraulic force is given to the piston
J	Jacobian matrix
K_a	Cylinder oil stiffness
K_b	Passive cylinder or damper oil stiffness
K_d	Piston stiffness of passive cylinder or damper
K_l	Link stiffness
K_p	Pushrod stiffness of the hydraulic actuator
K_s	Stiffness of table and specimen
K_{sp}	Specimen stiffness
M_p	Piston mass
M_t	Table and specimen mass
${}^{n}P_i$	Position vectors
${}^{i}R_{i-1}$	Rotation matrix
${}^{i-1}T_i$	Transformation matrix
x_n & z_n	Joint frames
Z_{max}	Total spring length
Z_p	Pushrod displacement
Z_t	Table displacement
$\dot{z}_{max}$	The first derivative of the total spring length
$\dot{z}_p$	The linear velocity of the pushrod
$\dot{z}_t$	The linear velocity of the table
$\ddot{z}_p$	Acceleration of pushrod
$\ddot{z}_t$	Acceleration of table
θ_n	The angle of the rotational joint
$\dot{\boldsymbol{\theta}}$	Joint rate vector
ζ	Damping ratio

Cite this article: A. X. Reni Prasad and M. Ganesh (2023). "Design, static analysis, and dynamic system modeling of 3-PPRS parallel manipulator with load-balancing UPS leg", Robotica **41**, 2735–2753. https://doi.org/10.1017/S0263574723000632